LA-UR- 10-08325

Approved for public release;
distribution is unlimited.

Title:	Second Order Multidimensional Sign-Preserving Remapping for ALE Methods
Author(s):	Ryan N. Hill J. Szmelter
Intended for:	NECDC Los Alamos, NM October 18-22, 2010

Form 836 (7/06)

Second Order Multidimensional Sign-Preserving Remapping for ALE Methods

[1]Hill R.N., [1]Szmelter J.
[1]*Loughborough University, Leicestershire, LE11 3TU, UK*
R.Hill2@lboro.ac.uk

A second-order conservative sign-preserving remapping scheme for Arbitrary Lagrangian-Eulerian (ALE) methods is developed utilising concepts of the Multidimensional Positive Definite Advection Transport Algorithm (MPDATA). The algorithm is inherently multidimensional, and so does not introduce splitting errors. The remapping is implemented in a two-dimensional, finite element ALE solver employing staggered quadrilateral meshes. The MPDATA remapping uses a finite volume discretisation developed for volume coordinates. It is applied for the remapping of density and internal energy arranged as cell centered, and velocity as nodal, dependent variables.

In the paper, the advection of scalar fields is examined first for test cases with prescribed mesh movement. A direct comparison of MPDATA with the performance of the van Leer MUSCL scheme indicates advantages of a multidimensional approach. Furthermore, distinctly different performance between basic MPDATA and the infinite gauge option is illustrated using benchmarks involving transport of a sign changing velocity field.

Further development extends the application of MPDATA remapping to the full ALE solver with a staggered mesh arrangement for density, internal energy and momentum using volume coordinates. At present, two options of the algorithm - basic and infinite gauge - are implemented. To ensure a meaningful assessment, an identical Lagrangian solver and computational mesh update routines are used with either MPDATA or van Leer MUSCL remapping. The evaluation places particular focus on the abilities of both schemes to accurately model multidimensional problems.

Theoretical considerations are supported with numerical examples. In addition to the prescribed mesh movement cases for advection of scalars, the demonstrations include two-dimensional Eulerian and ALE flow simulations on quadrilateral meshes with both fixed and variable timestep control. The key comparisons include the standard test cases of Sod and Noh for single material problems.

The results demonstrate that the MPDATA gauge option is suitable for providing accurate ALE remapping and preserves the multidimensionality and sign of both scalar and vector fields.

Prepared for Proceedings of the NECDC 2010

Introduction

Remapping within an arbitrary Lagrangian-Eulerian (ALE) scheme requires values of a scalar to be conservatively interpolated from one computational mesh to another which has differing geometry. Advection methods are typically utilised for the remapping phase, with fluxes being created by overlapping volumes between adjacent elements. This paper documents the application of MPDATA [1, 2] as a remapping scheme for this purpose.

In this study, the numerical tests initially follow Reference [3] and examine cases with prescribed mesh movement. Examples are extended to fields of varying sign - highlighting the benefits of the infinite gauge option of MPDATA [4]. Further development extends the application of MPDATA remapping to a complete ALE solver [5] with a staggered mesh arrangement for density, energy and momentum using volume coordinates, shown in Figure 1. In terms of accuracy, the ALE remapping scheme should be at least second order accurate, conservative, correctly deal with corner coupling errors in multiple dimensions and preserve symmetry when required. We investigate how MPDATA serves this purpose.

Demonstrations focus on the classical Noh problem. The problem is relevant to shock reflection and interactions, and has been extensively studied; refer to [6, 7] as well as the literature therein for in-depth analysis and reviews. In general, accurate solutions of the Noh problem can be obtained by methods based on the Eulerian framework, but simulations involving Lagrangian solutions introduce unphysical wall heating. ALE methods inherit errors introduced in the Lagrangian phase, which in turn raises an issue for the remapping phase. The remapping phase should accurately interpolate the Lagrangian solution, including all significant features of the variables, whether such features are deemed accurate or otherwise. In the case of the Noh problem, the wall heating features are unphysical, and should not be present in the solution. The remapping phase may then be employed to repair the solution in a computationally efficient manner. This study describes an MPDATA based treatment for reducing the wall heating errors in ALE/Lagrangian-Eulerian calculations, and highlights additional benefits of this treatment, such as the restoration of symmetry in multidimensional test cases.

MPDATA Based Remapping with Second-Order Filtering

In order to use MPDATA for remapping, it is useful to utilise the volume coordinate update of a scalar. For arbitrary flows, the volume update is given as

$$V^{(+)} = V^{(-)} - \Sigma_{k=1}^{4} \Delta V_k, \tag{1}$$

where ΔV_k denotes the quadrilateral generated by the movement of edge k from the post-Lagrangian mesh, denoted $^{(-)}$, to the remapped mesh, denoted $^{(+)}$. The scalar in each cell is given by its mean value over the cell volume, so that the corresponding scalar update is then

$$\psi^{(+)} = \frac{V^{(-)}\psi^{(-)}}{V^{(+)}} - \frac{1}{V^{(+)}} \Sigma_{k=1}^{4} \Delta V_k \psi_k^{(-)}. \tag{2}$$

Equation (2) corresponds to the first order upwind calculation required for MPDATA remapping. Upwind advection utilises a Courant number that is also required for the calculation of the pseudo velocities used to compensate the second order truncation error in MPDATA. Identification of the Courant number within (2) is therefore necessary for the subsequent steps in the algorithm.

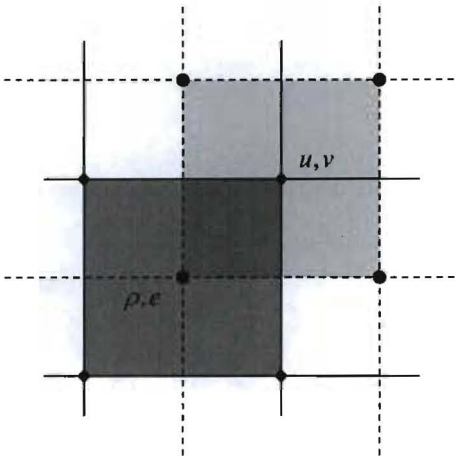

Figure 1: Illustration of the staggered grid arrangement. Density, ρ, and internal energy, e, are stored at element centres (circles) on the computational mesh (solid lines). Components of velocity, u and v, are stored at nodes (diamonds) which become the centres of elements on the dual mesh (dashed lines).

Defining $\Psi := V\psi$ and multiplying (2) by $V^{(-)}/V^{(-)}$, the scalar remapping becomes

$$\Psi^{(+)} = \Psi^{(-)} - \Sigma_{k=1}^{4} \frac{\Delta V_k}{V^{(-)}} \Psi_k^{(-)}, \tag{3}$$

which is now in the form of upwind advection used in [4], with $\Delta V_k/V^{(-)}$ being akin to the Courant number evaluated at edge k of an element. For consistency, the volume in the denominator of (3) is obtained by averaging over element volumes on either side of the edge. Repeating the update (2)-(3) using mass instead of volumes reveals that $\Delta V/V^{(-)}$ can be interpreted as the Courant number for all scalar and vector variables. The MPDATA scheme, generalised to volume coordinates including second-order filtering [8] is summarised below. Following [4], which provides the detailed derivation of MPDATA, only the volume coordinate extension is provided here, and to assist the reader, notation adopted from [4] is used.

By denoting the Courant number by $C = \Delta V/V^{(-)}$, the first pass is formulated as

$$\begin{aligned}
\Psi_{i,j}^{(1)} = \; & \Psi_{i,j}^{(-)} - \Big[F\left(\Psi_{i,j}^{(-)}, \Psi_{i+1,j}^{(-)}, C_{i+1/2,j}\right) - \beta_{i+1/2,j}\left(\Psi_{i+1,j}^{(-)} - \Psi_{i,j}^{(-)}\right) \\
& - F\left(\Psi_{i-1,j}^{(-)}, \Psi_{i,j}^{(-)}, C_{i-1/2,j}\right) - \beta_{i-1/2,j}\left(\Psi_{i,j}^{(-)} - \Psi_{i-1,j}^{(-)}\right) \Big] \\
& - \Big[F\left(\Psi_{i,j}^{(-)}, \Psi_{i,j+1}^{(-)}, C_{i,j+1/2}\right) - \beta_{i,j+1/2}\left(\Psi_{i,j+1}^{(-)} - \Psi_{i,j}^{(-)}\right) \\
& - F\left(\Psi_{i,j-1}^{(-)}, \Psi_{i,j}^{(-)}, C_{i,j-1/2}\right) - \beta_{i,j-1/2}\left(\Psi_{i,j}^{(-)} - \Psi_{i,j-1}^{(-)}\right) \Big],
\end{aligned} \tag{4}$$

where half integer index subscripts indicate edge (and nodal) centred variables, and integer indices denote

element centred variables. The flux function F is defined as

$$F\left(\Psi_a, \Psi_b, C\right) \equiv \frac{1}{2}\left(C + |C|\right)\Psi_a + \frac{1}{2}\left(C - |C|\right)\Psi_b.$$

Terms utilising the small positive coefficient β are activated when oscillations are present in the first-order solution and may be filtered.

The pseudo velocities (antidiffusive overlap volumes), modified into antidiffusive Courant numbers for the second pass are

$$C^{(1)}_{i+1/2,j} \equiv \left(\left|C_{i+1/2,j}\right| - \left(C_{i+1/2,j}\right)^2 + 2\beta_{i+1/2,j}\right) A^{(1)} - C_{i+1/2,j}\bar{C}_{i+1/2,j}B^{(1)}, \tag{5}$$

where $\bar{C}_{i+1/2,j} = 1/4\left(C_{i,j+1/2} + C_{i,j-1/2} + C_{i+1,j+1/2} + C_{i+1,j-1/2}\right)$, with an analogous expression for $C^{(1)}_{i-1/2,j}$, and

$$C^{(1)}_{i,j+1/2} \equiv \left(\left|C_{i,j+1/2}\right| - \left(C_{i,j+1/2}\right)^2 + 2\beta_{i,j+1/2}\right) B^{(1)} - \bar{C}_{i,j+1/2}C_{i,j+1/2}A^{(1)}, \tag{6}$$

where $\bar{C}_{i,j+1/2} = 1/4\left(C_{i+1/2,j} + C_{i-1/2,j} + C_{i+1/2,j+1} + C_{i-1/2,j+1}\right)$, with an analogous expression for $C^{(1)}_{i,j-1/2}$; where

$$A^{(1)} \equiv \left[\frac{\delta x}{2\psi}\frac{\partial \psi}{\partial x}\right]^{(+)}_{i+1/2,j} = \frac{\left|\psi^{(1)}_{i+1,j}\right| - \left|\psi^{(1)}_{i,j}\right|}{\left|\psi^{(1)}_{i+1,j}\right| + \left|\psi^{(1)}_{i,j}\right|}, \tag{7}$$

$$B^{(1)} \equiv \left[\frac{\delta y}{2\psi}\frac{\partial \psi}{\partial y}\right]^{(+)}_{i+1/2,j} = \frac{1}{2}\frac{\left|\psi^{(1)}_{i+1,j+1}\right| + \left|\psi^{(1)}_{i,j+1}\right| - \left|\psi^{(1)}_{i+1,j-1}\right| - \left|\psi^{(1)}_{i,j-1}\right|}{\left|\psi^{(1)}_{i+1.j+1}\right| + \left|\psi^{(1)}_{i,j+1}\right| + \left|\psi^{(1)}_{i+1,j-1}\right| + \left|\psi^{(1)}_{i,j-1}\right|}. \tag{8}$$

The corrective pass then takes the following form,

$$\begin{aligned}\Psi^{(+)}_{i,j} = \; & \Psi^{(1)}_{i,j} - \left[F\left(\Psi^{(1)}_{i,j}, \Psi^{(1)}_{i+1,j}, C^{(1)}_{i+1/2,j}\right) - F\left(\Psi^{(1)}_{i-1,j}, \Psi^{(1)}_{i,j}, C^{(1)}_{i-1/2,j}\right)\right] \\ & - \left[F\left(\Psi^{(1)}_{i,j}, \Psi^{(1)}_{i,j+1}, C^{(1)}_{i,j+1/2}\right) - F\left(\Psi^{(1)}_{i,j-1}, \Psi^{(1)}_{i,j}, C^{(1)}_{i,j-1/2}\right)\right],\end{aligned} \tag{9}$$

The infinite gauge (whereby the algorithm is linearised around an arbitrarily large constant) and monotonic options used within the remapping in this paper are detailed in [4] and [2] respectively.

Prescribed Mesh Movement Test Cases

A key aspect of the ALE method is to remap the post-Lagrangian solution onto a relaxed mesh which will have improved geometric properties. The prescribed mesh movement test cases proposed by Margolin and Shashkov [3] are designed to test the performance of the remapping schemes for this purpose. The test

cases remap initial distributions of a positive scalar field on to a series of meshes where nodal positions are determined by a tensor product function. The scalar field is mapped from a mesh at time t^n to the prescribed mesh at time t^{n+1}, with the overlap volumes calculated using the two nodal positions of an element edge on the mesh at times t^n and t^{n+1}. The nodal positions are purposely specified to ensure that the overlap volumes do not cover more than one element [9], thus maintaining consistency with the CFL condition in an ALE scheme.

In the following example, the tensor product meshes are generated in the domain $[0,1] \times [0,1]$ using the functions

$$x(\xi,\eta,t) = (1-\alpha(t))\xi + \alpha(t)\xi^3, \quad y(\xi,\eta,t) = (1-\alpha(t))\eta + \alpha(t)\eta^2, \tag{10}$$

$$\alpha(t) = \frac{sin(4\pi t)}{2}, \tag{11}$$

to give the x and y coordinates of the nodes in the computational mesh, with

$$0 \leq \xi \leq 1, \;\; 0 \leq \eta \leq 1, \;\; 0 \leq t \leq 1\,.$$

The parameters ξ and η are discretised according to the expressions

$$\xi_i = \frac{i-1}{i_{max}-1}, \;\; i = 1,\ldots,i_{max}; \qquad \eta_j = \frac{j-1}{j_{max}-1}, \;\; j = 1,\ldots,j_{max},$$

at the time level t^n determined by

$$t^n = \frac{n}{n_{max}}, n = 0,\ldots,n_{max}\,,$$

to give a sequence of meshes $\left\{x^n_{i,j}\right\}$ given by

$$x^n_{i,j} = x(\xi_i,\eta_j,t^n), \qquad y^n_{i,j} = y(\xi_i,\eta_j,t^n). \tag{12}$$

The indices i and j correspond to the nodes of the mesh, with $i_{max} = j_{max} = 129$ and $n_{max} = 640$ in the test cases shown. The tensor product movement (10)-(12) has the effect of skewing the mesh from an initially regular grid ($t = t^0 = 0, \alpha(t) = 0$) before returning to a regular mesh ($t = t^n = 1, \alpha(t) = 0$).

An initial test case, illustrated in Fig. 2, is performed featuring a discontinuity (normal shock) in a positive scalar variable given by (13). This function essentially represents one-dimensional transport between elements with both the van Leer and MPDATA methods performing well.

$$\psi\,(x,y) = \begin{cases} 1 & \text{if } x > 0.5, \\ 0 & \text{if } x \leq 0.5. \end{cases} \tag{13}$$

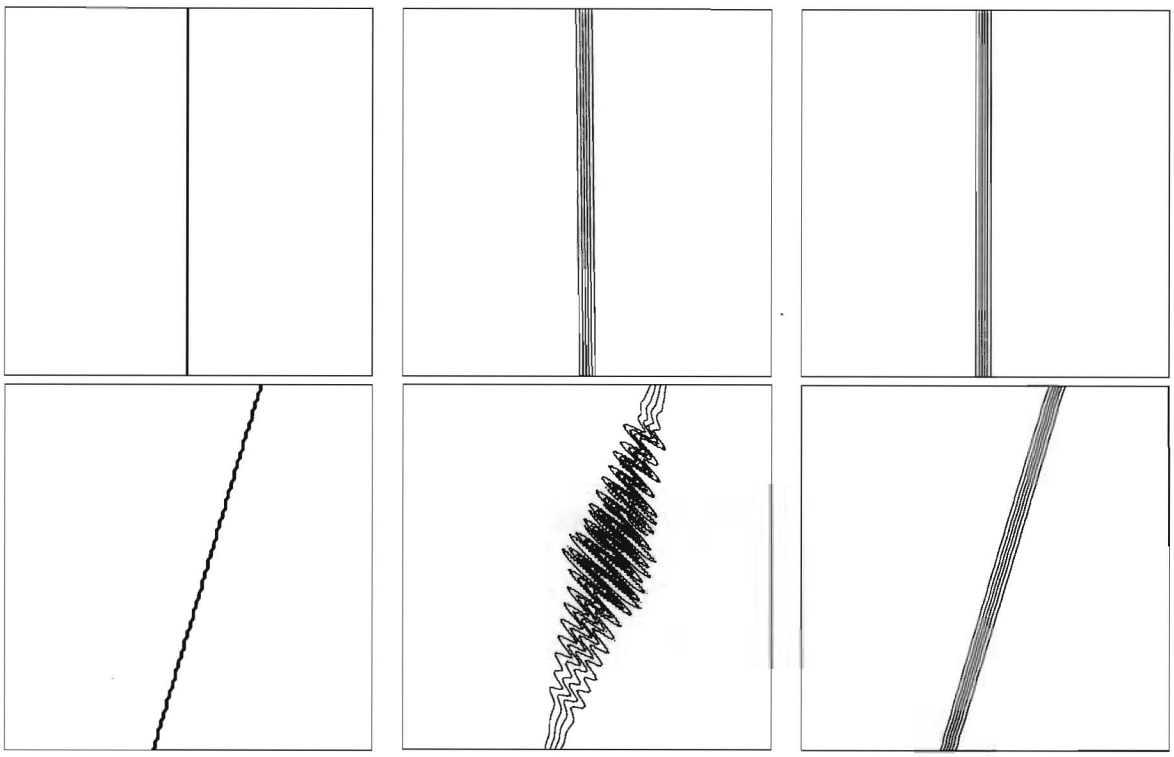

Figure 2: Isolines at $t = t^{n_{max}}$ for a normal (top) and oblique (bottom) shock remapped over tensor product mesh movement. The contour interval is 0.25, minimum contour level, 0.0. The exact solution (left plate) and the solutions given by the van Leer and MPDATA based remapping schemes (centre and right plates respectively)

A more rigorous test case features an oblique shock function, detailed in (14). It involves transport between diagonal elements and tests the multidimensional capabilities of the remapping schemes. Fig. 2 shows the exact, van Leer and MPDATA solutions in the left, centre and right plates respectively. Limitations of the one dimensional basis of the isotropic remapping van Leer based scheme are again highlighted, with undesired rippling introduced into the solution as a result of the inadequate corner coupling. The MPDATA remapping however, deals with the corner transport effectively, gives results consistent with the exact values (14), and appears to improve on both the MPDATA inspired Positivity-preserving Error Compensation Algorithm and the Barth-Jespersen solutions given in [3].

$$\psi(x,y) = \begin{cases} 1.0 & \text{if } y > (x-0.4)/0.3, \\ 0.0 & \text{if } y \leq (x-0.4)/0.3. \end{cases} \tag{14}$$

The shock distributions involve non-negative distributions. To allow further analysis of the remapping

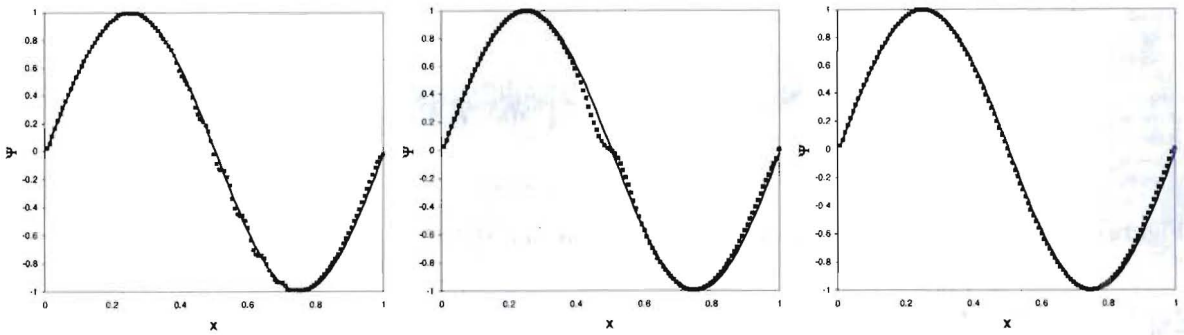

Figure 3: Profiles of the 'sine' distribution through $x = 0.25$ after 640 pseudo timesteps. Left: Isotropic van Leer, center: MPDATA, Infinite gauge MPDATA.

methods, a distribution featuring a smooth sign changing distribution is proposed:

$$\psi(x, y) = sin(2\pi x)sin(2\pi y). \tag{15}$$

MPDATA was originally derived for non-negative scalar and vector fields, and subsequently extended to positive or negative fields, cf. Section 3.2 in [4]. This extension utilises absolute values in the calculations of derivatives in the pseudo velocity calculation. However, for some test cases involving fields of varying sign, aspects of the solution may not be accurate. For example, if $\psi_{i,j} \approx -\psi_{i+1,j}$ then $\partial\psi/\partial\mathbf{x} \rightarrow \pm\infty$ as $\psi_{i,j}$ increases in magnitude with $-\psi_{i+1,j}$, whereas $\partial\left|\psi\right|/\partial\mathbf{x} \rightarrow 0$. The infinite gauge option of MPDATA is an alternative approach to generalising MPDATA to fields of varying sign.

The volume coordinate infinite gauge option is obtained by linearising the algorithm (4)-(9) around an arbitrarily large constant, see Section 4 in [10] for a detailed discussion of the process. In this way, the scalar or vector field is modified to be effectively non-negative, which in turn removes the need to exploit absolute values in derivatives. In practice, the basic algorithm is altered such that unity replaces each Ψ in the denominators of (7) and (8), and in the fluxes of the corrective pass (9).

Figure 3 shows a cut through the distribution along $x = 0.25$. The isotropic van Leer scheme, shown for comparison, struggles with the mesh movement, and as a result introduces undesired ripples similar to those reported in [15] which dominate the solution (particularly along the profile $x = 0.5$, not shown). In contrast, the basic MPDATA solution correctly remaps the scalar, with the exception of regions where the distribution changes sign because $\partial\left|\psi\right|/\partial\mathbf{x} \rightarrow 0$. In this case, an unphysical reduction in the gradient of the scalar distribution is introduced. Such errors are not present in the infinite gauge MPDATA solution, with correct remapping achieved for all values. Scalar conservation during the MPDATA gauge calculation, using the error norm

$$\epsilon = \frac{\sum_{i,j}\Psi_{i,j}^{(+)} - \sum_{i,j}\Psi_{i,j}^{(-)}}{\sum_{i,j}\Psi_{i,j}^{(-)}} \tag{16}$$

after each pseudo time step, is shown in Figure 4.

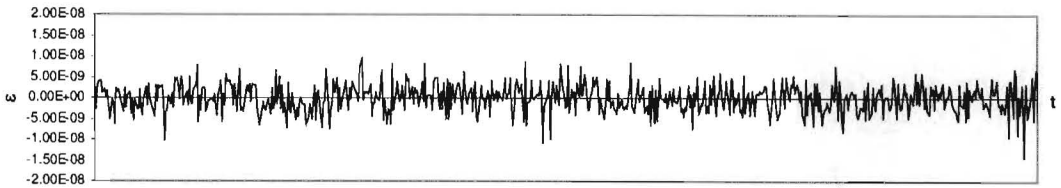

Figure 4: Temporal evolution of the conservation error for MPDATA gauge remapping.

The Explosion Problem

The Explosion problem [11] is essentially an axisymmetric two dimensional extension to Sod's shock tube benchmark. The domain is filled with an ideal gas with specific heat ratio coefficient $\gamma = 1.4$. A circular region of radius $r = 0.4$ is centred at the origin of a $[-1, 1] \times [-1, 1]$ domain with higher density, ρ, and pressure, p, compared to the rest of the domain.

$$\rho = \begin{cases} 1 & \text{if } |r| \leq 0.4, \\ 0.125 & \text{if } |r| > 0.4. \end{cases} \qquad p = \begin{cases} 1 & \text{if } |r| \leq 0.4, \\ 0.1 & \text{if } |r| > 0.4. \end{cases}$$

The gas is initially at rest so that a contact discontinuity, shock and rarefaction wave are formed radially as the simulation progresses. The computations are conducted on 100×100 and 200×200 Cartesian grids with Eulerian and Winslow equipotential [12] rezoning. The geometry of the Cartesian grid is mismatched with the radial initial conditions which may evoke perturbations at the interface between regions of high and low densities and pressures.

A comparison of the resulting density contours at $t = 0.25$ is shown in Fig. 5. A considerable error is visible in the rarefaction wave of the van Leer solution using isotropic remapping. Indeed, this arises due to the castellated interface between material properties where the lack of true multidimensionality highlights corner coupling errors. Significantly, the errors seeded at the initial material interface are impinging upon the radial position of the contact discontinuity. This has the result of damaging the required symmetry in the simulation. The MPDATA based scheme however, does not exhibit the same behaviour at the material interface, with the castellation effect being suppressed due to the utilisation of information from all directions in the remapping. Preservation of symmetry is therefore stronger in the MPDATA scheme. Such a mismatch of geometries may be reduced by smoothing the interface using area weighting in the cells which are intersected by the circle. The initial castellated interface is retained however to provide a challenge when studying properties of remapping. As seen in Fig. 5, the solutions obtained with both rezone strategies show similar features with the results from the full ALE calculation being more accurate.

The density, energy, pressure and velocity profiles representing a cut through the 200×200 mesh at $45°$ are shown in Fig. 6. Both methods perform comparably in each of the profiles, and conform to results in the literature, for example the high order one dimensional solution of Toro (Fig. 17.4 in [11]). It can be seen that the isotropic remapping van Leer scheme introduces an overshoot in the velocity profile in the region surrounding $r = 0.4$ which is linked to a dip at the base of the rarefaction wave of the density profile. This feature is not physical, and is not present in the MPDATA solution. Small inaccuracies at the contact discontinuity and shock are present within the profiles for both solutions. The van Leer solution

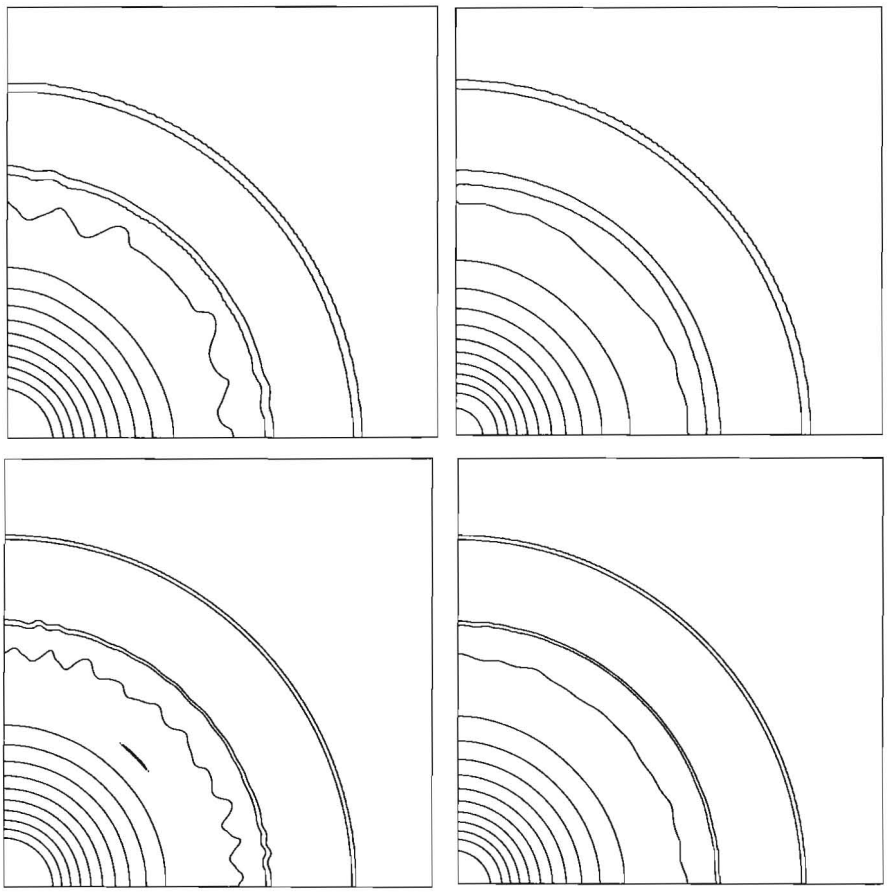

Figure 5: Density contours at $t = 0.25$ for the Explosion problem with Eulerian (left) and Winslow (right) mesh rezoning; the van Leer scheme is shown in the upper plates, and the infinite gauge MPDATA scheme in the lower plates. The contour interval is 0.066, minimum contour level, 0.125.

using Strang splitting appears to be more diffusive in the regions of discontinuities, however, a rigorous comparison of this result is impeded by differences in the implementation of the routines used in ALE.

The Noh Problem

The Noh problem [6] consists of a cold, ideal gas with density $\rho = 1.0$, internal energy $e = 0.0$, ratio of specific heat $\gamma = \frac{5}{3}$ and uniform velocity $\|\mathbf{v}\| = -1.0$ forcing the gas into a rigid wall. An infinite strength shock is generated at the wall boundary and travels in the opposite direction to the gas flow. The simulation of the planar case (rigid wall along $x = 0.0$) is performed in a $[0, 1] \times [0, 0.2]$ domain, discretised with a series of uniform resolution grids. The simulation of the cylindrical case (wall at $(x, y) = (0, 0)$) is performed on a Cartesian mesh on a $[0, 1] \times [0, 1]$ domain, with 200×200 elements, and $\Delta t = 0.0005$. Exact values are used on inflow boundaries, with symmetry utilised on boundaries $x = 0$ and $y = 0$ in the cylindrical case. Both planar and cylindrical cases use a constant time step, terminating at time $t = 0.6$.

The wall heating error in the Noh problem arises in the Lagrangian solution of unsteady wave propagation and is related to factors such as the application of artificial viscosity, phase errors, wave speed or changes in mesh resolution travelling with the shock. A thorough analysis of the sources of wall heating is provided in Reference [7]. Due to the nature of the Noh problem, a strong shock is formed next to an impermeable wall. At this stage, elements near the boundary experience large compression so that the added artificial viscosity cannot be dissipated sufficiently, manifesting itself as unphysical heating. This generates a build up of energy at the wall boundary which in turn forces a drop in the density as the equation of state establishes the correct pressure level. Herein, properties of the MPDATA based remapping are exploited to regulate the solution.

By design, MPDATA relies on the iterative application of the upwind scheme, where subsequent iterations compensate for the implicit viscosity of the preceding steps. Thus it bears an analogy to generalised similarity models, where an estimate of the full unfiltered Navier-Stokes velocity (that enters the subgrid-scale stress tensor) is obtained by an approximate inversion of the filtering operation, i.e. deconvolution [1]. Building upon this concept, and in the spirit of Flux Corrected Transport methods [13], additional diffusion i.e. activating β terms in (4)-(6) may be explicitly added to the first upwind iteration to remove oscillations in the first-order solution. The second iteration, (9), compensates the truncation error of the first step (4) which includes the added dissipation. With $\delta t \propto \delta x$, the explicit diffusion enters (4) as an $\mathcal{O}(\delta x)$ correction, whereupon its reversal in the corrective step leaves an $\mathcal{O}(\delta x^2)$ residual; see [8] for a thorough exposition. Similarly to MPDATA, this treatment is fully multidimensional.

Within the second-order filtering option, $\beta = 0.02$ is the default value, but may vary in space or be set to zero upon the detection of a shock (discontinuity). The effective level of diffusion is an order of magnitude lower than that reported in [13]. Wall heating errors will be the focus of this study, with preservation of symmetry receiving attention in the cylindrical case.

Planar Case

The left plate of Fig. 7 shows the density profile for the van Leer and MPDATA-gauge ($\beta = 0.0$) schemes. It can be seen in this diagram that the MPDATA result is correctly aligned to the exact solution in terms of the shock position ($x = 0.19958$ using linear interpolation for $\rho = 2.5$) and the level of post-shock density accumulation, whereas the van Leer scheme incorrectly aligns both features (shock at $x = 0.19073$) in a

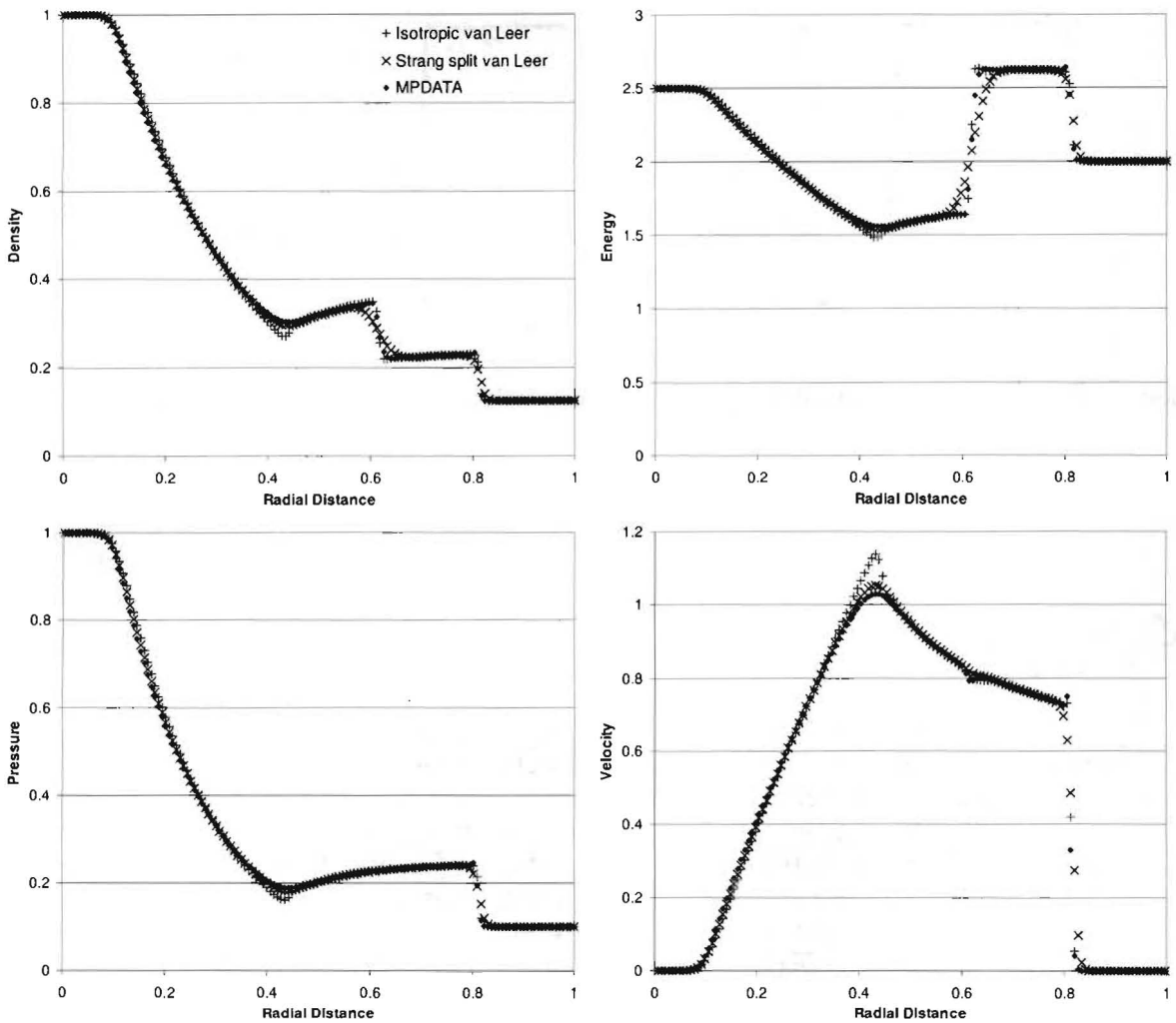

Figure 6: Density, energy, pressure and velocity profiles of the Explosion problem with Eulerian rezoning.

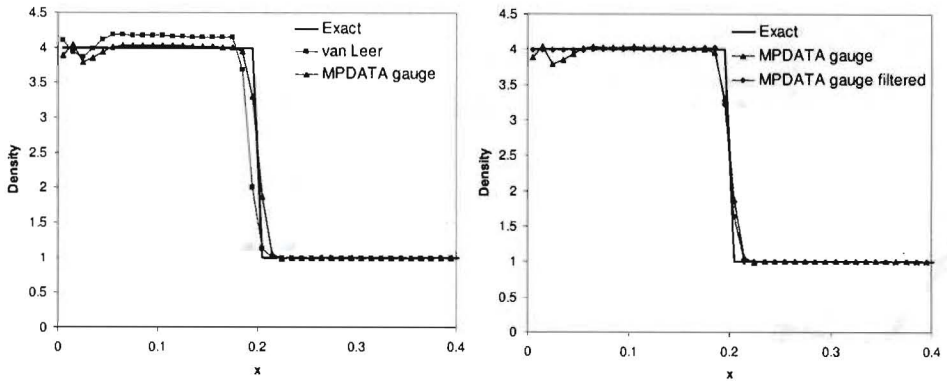

Figure 7: Density profiles of the planar case of the Noh problem ($400 \times 20, \Delta t = 0.00025$).

	Grid	Density	I.E.	T.E.	Pressure	Velocity
van Leer	100×20	0.105941	0.148222	0.148211	0.186724	0.079659
	200×20	0.126266	0.188564	0.188557	0.203178	0.094454
	400×20	0.139633	0.208208	0.208204	0.212429	0.102806
MPDATA	100×20	0.058166	0.064287	0.064252	0.074276	0.035359
	200×20	0.040818	0.043834	0.043832	0.058089	0.025558
	400×20	0.030565	0.035261	0.035260	0.053451	0.021844
MPDATA	100×20	0.056939	0.061482	0.061475	0.075888	0.035611
filtered	200×20	0.039963	0.042083	0.042081	0.057768	0.025556
	400×20	0.029813	0.033872	0.033871	0.053052	0.021781

Table I: L_2 error data for planar Noh problem with increasing mesh resolution in the direction of flow. I.E. denotes internal energy; T.E., total energy.

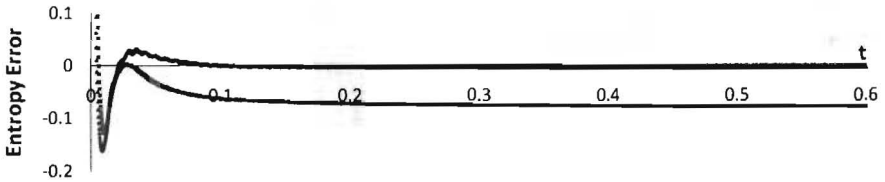

Figure 8: Entropy errors for the planar Noh Problem ($400 \times 20, \Delta t = 0.00025$)**. van Leer (pink square), MPDATA gauge (blue triangle), MPDATA gauge filtered (red diamond).**

manner consistent with results shown in [7] for Eulerian calculations using internal energy.

The van Leer scheme has masked the wall heating error. This feature has arisen due to the van Leer scheme being forced to give a first-order accurate solution at the wall elements because the larger stencil required to construct the monotonic piecewise linear distribution of the transported variables is not available at the boundary. The MPDATA based scheme has accurately remapped the Lagrangian wall heating features, which are unphysical, near the boundary at $x = 0.0$, therefore a self-regulating application of small explicit dissipation of wall heating errors is beneficial. This is achieved with the second-order filtering option ($\beta = 0.02$ for density and internal energy remapping) which removes the build up of energy at the boundary.

The filtering option of MPDATA is applied anisotropically in the direction of flow at all element edges except those where a shock has been detected. Therefore, the filtering does not smear the shock any further than has been done so with the application of artificial viscosity in the Lagrangian phase, and gives a more accurate shock position ($x = 0.19961$). The shock is detected automatically by examination of pressure gradients. The exclusion of the shock from the filtering is not essential, but provides a modest enhancement.

The behaviour, illustrated in Figure 7, of all schemes is consistent across coarse and finer resolution meshes. The departures from the exact solutions are reflected by Table I which gives L_2 error data for $100 \times 20, 200 \times 20$ and 400×20 meshes. These norm values show consistently higher errors in all variables for the van Leer scheme compared to the MPDATA based scheme. Due to the presence of a shock, the treatment of inflow boundaries and other factors, Table I is not suitable for an assessment of asymptotic mesh convergence. A second order asymptotic mesh convergence study of MPDATA remapping was conducted in [15] for a pure advection test with prescribed mesh velocity.

Solutions using the internal energy equation depend upon the level of entropy production. Fig. 8 shows the ratio of entropy error (defined in [7]) for each method. All methods have large start up errors (maximum entropy error for the van Leer scheme is 1.652, MPDATA based schemes, 1.655), however the van Leer scheme stabilises to a level significantly below the correct production level so that the incorrect features are evident. The MPDATA solutions attain more accurate levels of entropy production, however it can be seen that the start up errors and the conservation of internal energy rather than total energy, cf. [7, 8], are still affecting the solutions. This is seen by the MPDATA-based remapping entropy errors asymptotically approaching a negative value (-0.006 at $t = 0.6$).

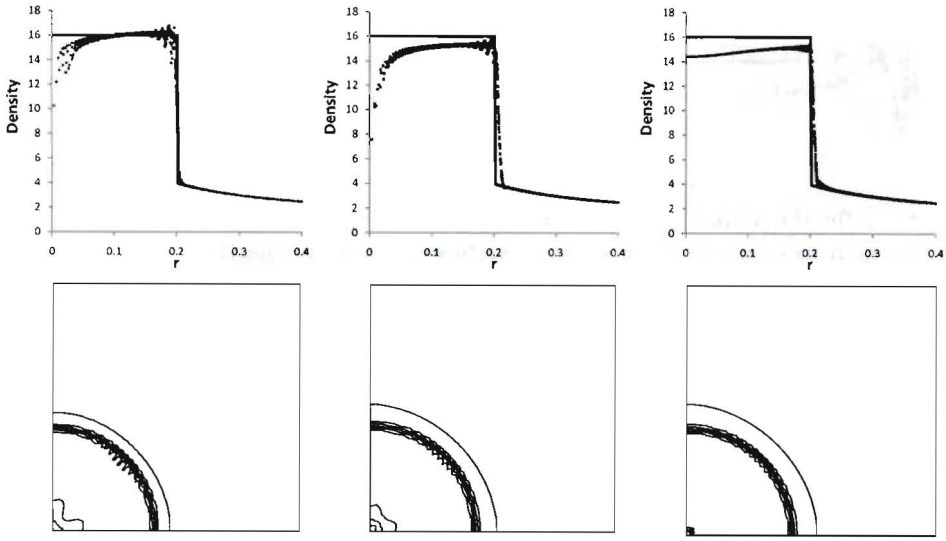

Figure 9: Upper row: Density plotted against radius for the cylindrical case of the Noh problem (Cartesian mesh). Left: van Leer, centre: MPDATA gauge, right: MPDATA gauge with second order filtering. Lower row: Corresponding density contours (quarter of the domain shown), minimum value $\rho = 2.0$, contour interval, 1.0.

Cylindrical Case

Figure 9 shows the density distributions obtained on a 200×200 Cartesian mesh at $t = 0.6$ ($\Delta t = 0.0005$). The van Leer based scheme is extended to two-dimensions by isotropic remapping. In this case corner coupling errors dominate the van Leer solution with a loss of symmetry, and significant errors along the cut $x = y$ (linearly interpolated shock position along for $\rho = 10$ at $r = 0.19932$)[1]. As in the planar case, the method features a first-order solution at the "wall" (origin), however in this case the first-order solution does not mask the wall heating errors. The MPDATA gauge solution features an incorrect shock position ($r = 0.20646$) because of the wall heating errors. This in turn leads to an under evaluation of post-shock density accumulation. The multidimensional nature of MPDATA provides greater preservation of symmetry, with a significant reduction in errors along the cut $x = y$, as highlighted in the contour plots of Fig. 9.

Applying the second-order filtering with MPDATA gauge significantly reduces the wall heating errors, and improves the preservation of symmetry. However, the effect of filtering is ultimately limited by the underlying Lagrange and MPDATA gauge solution, so that the shock position ($r = 0.20544$) and post-shock density accumulation are improved, but not fully regulated to the correct levels. The key result from the second-order filtering solution in the cylindrical case is the marked improvement in symmetry.

[1] A multidimensional isotropic extension of any one-dimensional scheme is not optimal. A scheme in which a one-dimensional version of MPDATA was employed isotropically in place of the van Leer scheme produced results (not shown) very close to those in the left panel of Fig. 9

Christensen [14] monotonic artificial viscosity is used in Lagrangian phase of the simulations, with coefficients $c_q = 0.75$ and $c_l = 0.5$. The c_l coefficient determines the diffusivity of the artificial viscosity. A reduction of this coefficient results in oscillations along the post shock density accumulation, and is therefore not appropriate for unfiltered methods. The filtering option however, introduces a small amount of diffusion in the remapping phase, and in this case c_l may be reduced, with c_q remaining unchanged (not shown). In the planar case, this permits very low wall heating errors on coarse meshes. In the cylindrical case, greater symmetry preservation is provided due to a reduction of oscillations in the post-shock region near the jump in density, particulary along the cut $x = y$.

Conclusions

A second-order accurate MPDATA remapping has been presented. The work builds upon developments of the algorithm for ALE calculations shown in [15, 16]. Conservativity and beneficial properties of the infinite gauge option for MPDATA based remapping have been discussed. The infinite gauge option has been shown to correctly deal with distributions containing a change in sign. This property affirms the conclusions obtained in [15, 16] stating that the infinite gauge option offers greater accuracy and flexibility compared to the basic MPDATA for remapping. Improvements in the accuracy of remapped solutions is also obtained by exploiting the properties of MPDATA to preserve symmetry and to remove wall heating errors

MPDATA has shown the ability to retain second order accurate calculations for elements along the wall (or potentially, a material) boundary. The capability of the MPDATA based remapping scheme to correctly remap the Lagrangian features at the wall boundary (with or without second-order filtering) is particularly desirable for the application of MPDATA based methods in future multimaterial ALE simulations, in which case the material boundary will have properties similar to a wall boundary.

Acknowlegements:

Discussions with Andrew J. Barlow and Robert Kevis are gratefully acknowledged. This work was supported by the Atomic Weapons Establishment (AWE), Aldermaston.

References

[1] Smolarkiewicz PK. Multidimensional Positive Definite Advection Transport Algorithm: An Overview. Int J Numer Methods Fluids 2006;50:1123-44.

[2] Smolarkiewicz PK, Szmelter J. MPDATA: An edge-based unstructured-grid formulation. J Comp Phys 2005;206:624-49.

[3] Margolin LG, Shashkov M. Second-order sign-preserving conservative interpolation (remapping) on general grids. *Journal of Computational Physics* 2003; **184**:266–298.

[4] Smolarkiewicz PK, Margolin LG. MPDATA: A finite-difference solver for geophysical flows. J Comp Phys 1998;140:459-80.

[5] Barlow AJ. A compatible finite element multi-material ALE hydrodynamics algorithm. Int J Numer Methods Fluids 2008;56:953-64.

[6] Noh WF. Errors for calculations of strong shocks using an artificial viscosity and an artificial heat flux. J Comp Phys 1987;72:78-120.

[7] W.J. Rider. Revisiting Wall heating, J Comp Phys 2000;162:395-410.

[8] Smolarkiewicz PK, Szmelter J. Iterated Upwind Schemes for Gas Dynamics. J Comp Phys 2009;228:33-54.

[9] Benson DJ. Computational methods in Lagrangian and Eulerian hydrocodes. Comput Meth Appl Mech Eng 1992;99:235-394.

[10] Smolarkiewicz PK, Clark TL. The Multidimensional Positive Definite Advection Transport Algorithm: Further Development and Applications. J Comp Phys 1986;67:396-438.

[11] Toro EF. *Riemann Solvers and Numerical Methods for Fluid Dynamics*. 2nd Edition, Springer, 1999.

[12] A.M. Winslow, Equipotential zoning of two-dimensional meshes, Lawrence Radiation Laboratory, UCRL-7312, 1963.

[13] S.T. Zalesak. A fully multidimensional flux-corrected transport algorithm for fluids, J Comp Phys 1979;31:335-62.

[14] R.B. Christensen. Godunov Methods on a Staggered Mesh - An Improved Artificial Viscosity. Technical Report UCRL-JC-105269 Preprint, Lawrence Livermore National Laboratory, 1990.

[15] R.N. Hill and J. Szmelter. A multidimensional positive definite remapping algorithm for arbitrary LagrangianEulerian methods, *International Journal for Numerical Methods in Fluids*, in press, DOI: 10.1002/fld.2351.

[16] R.N. Hill and J. Szmelter. A multidimensional positive definite remapping for Lagrangian solutions of the Noh problem. *Computers and Fluids*, in press, doi:10.1016/j.compfluid.2010.09.007.